Triplet Exciton and Trap States in the Charge-Transfer Crystal Anthracene/Tetrachlorophthalic Anhydride (A/TCPA)

W. Mühle, J. Krzystek *, J. U. von Schütz, and H. C. Wolf

3. Physikalisches Institut, Universität Stuttgart

Z. Naturforsch. **44a**, 610–624 (1989); received April 19, 1989

Mobile triplet excitons in A/TCPA have been detected from 1.2 to 300 K via ESR and zero-field ODMR. Their features such as linewidth and zero-field-splitting (zfs) parameters are discussed in terms of the temperature-dependent crystal structure. Between 1.2 and 4.2 K the excitons are caged by barriers. When raising the temperature a thermally activated hopping takes place between two triplet bands separated by 40 cm^{-1}, having different zfs parameters $|D_A| = 2126.5$, $|E_A| = 241.0$, $|D_B| = 2112.5$, $|E_B| = 238.0$ MHz and different zfs tensor orientations. Above 100 K an increase of the librations of the anthracene molecules broadens the homogeneous excitonic lines. The homogeneous linewidth is measured by the free induction decay. The CT character of the triplet state is estimated as $c_{CT}^2 \leqq 4\%$.

1. Introduction

The presence of two triplet bands discovered in A/TCPA [1] is a feature found in certain molecular crystals, like dibromonaphthalene [2] whose structure consists of two sublattices. It is, however, uncommon in 1:1 CT-crystals, and the origin of the two bands in A/TCPA was not clear. Also, the manifold of magnetic resonance results obtained in the past could be only partially understood until now. With the successful determination of the temperature-dependent crystal structure, which revealed two nonequivalent stacks and two phase transitions [1], the magnetic properties of the triplet state were reexamined as a function of temperature in detail.

The following questions were raised:

- Can one detect triplet excitons in both types of stacks?
- Is the motion of the excitons restricted to the stack of excitation?
- What is the difference between the magnetic properties of bands "A" and "B"?
- Does interband interaction take place, and is this reflected in lineshape, position and dynamics of the mobile excitons?
- Are these excited states neutral (local) or is some charge transfer involved?

Some of these questions have been answered by our previous experiments rather intuitively [3, 4]. This work brings answers to some of the previously encountered problems. Especially, the time behavior of zero-field ESR and ODMR signals after pulsed microwave excitation solves the question of their homogeneity. Within the time-resolved experiments the first successful detection of the free induction decay (FID) of a triplet exciton in zero magnetic field is of particular importance, and so is the continuous detection of the cw-ESR and -ODMR excitonic signals from the lowest up to room temperature.

2. Experimental

2.1. ODMR and ESR Spectroscopy

The equipment used in our cw-ODMR and -ESR experiments has been described in [5] with the exception of the following details:

- a Spectra Physics 164-03/375 dye laser pumped by an argon-ion laser was used to provide direct triplet population in some of the experiments,
- in time-resolved ODMR experiments microwave were pulsed using with PIN-diode switches (HP 33104 A and 33124 A, switch time 50 ns, or General Microwave DM 863 BH, switch time max. 10 ns) combined with a home-built pulse generator.

The zero-field pulsed ESR apparatus was designed in principle after [6]. Its central point was a coaxial reentrant type resonator first described in [7] which had the advantage of good tunability together with

* Institute of Physics, Polish Academy of Sciences, Al. Lotnikow 32, PL-02668 Warsaw, Poland.

Reprint requests to Prof. H. C. Wolf, 3. Physikalisches Institut, Universität Stuttgart, Pfaffenwaldring 57, D-7000 Stuttgart 80.

0932-0784 / 89 / 0700-0610 $ 01.30/0. – Please order a reprint rather than making your own copy.

small dimensions in relation to the wavelengths ($\nu_{rf} = 1.2$–4.5 GHz). Optical excitation was achieved through a hole in the side wall of the resonator. The crystal was mounted on the end of a quartz rod acting also as a lightguide for collecting the emitted radiation in ODMR experiments performed in the resonator instead of the standard helix. The Q-factor was 100–500. The resolution in the time domain, which is determined by the dead-time of the receiver was of the order of 0.5 μs.

2.2. Crystal Growing

The A/TCPA crystals were grown from zone-refined components using three independent methods: Bridgman, solution, and plate-sublimation. The crystals thus obtained were examined by mass spectroscopy with the result of no significant differences in their purity. In all cases a main impurity of the mass of carbazole could be detected in a concentration of 1×10^{-4} mole/mole.

The morphology and dimensions of the yellow-orange A/TCPA crystals depend on the growth method. For the solution-grown specimens the typical dimensions were $0.5 \times 0.5 \times 1.5$ mm^3, the shape was needle-like with at least 6 cleavage planes discernible. The sublimation-grown cystals were similar in shape and dimensions, while the Bridgman-grown ones were bigger but with an ill-defined morphology.

DSC (differential scanning calorimetry) measurements have revealed phase transitions at $T = 257$ K [8] (coinciding with a jump in the proton spin lattice relaxation [9]) and at $T = 194 \pm 4$ K.

2.3. Crystal Structure

The crystal structure of A/TCPA will be presented in detail in [1]. For this work, the following features are relevant:

- there are three distinct phases separated by two phase transitions at 194 and 257 K,
- in the low-temperature phase (below 194 K) there are four complexes in the unit cell, two of which are unrelated by any symmetry operation and so energetically nonequivalent,
- in the medium-temperature phase ($194 < T < 257$ K) the number of complexes in the unit cell is preserved but the TCPA molecules in the stacks are randomly distributed over two possible orientations.
- in the high temperature phase (above 257 K) the size of the unit cell is reduced by a factor of two and there are two complex pairs in the unit cell; the TCPA molecules are disordered as before,
- the molecules undergo thermally activated librations within a small angular range (max. 4.4° at 230 K for anthracene; at higher temperatures the molecules are no more rigid).

3. Results

3.1. CW-ODMR

Our studies are based on the preliminary results presented in [3] and show that the ODMR spectrum significantly depends on the excitation and detection conditions (Figure 1). We distinguish between excitation above the S_1 origin at $\bar{\nu} = 20660$ cm^{-1} (into the S_1-band) and below the S_1-origin into the trap manifold [3].

3.1.1. F-ODMR

The F_2-ODMR signals from Fig. 1 appearing when exciting above the S_1 origin were reproduced in higher resolution and with a better signal-to-noise ratio,

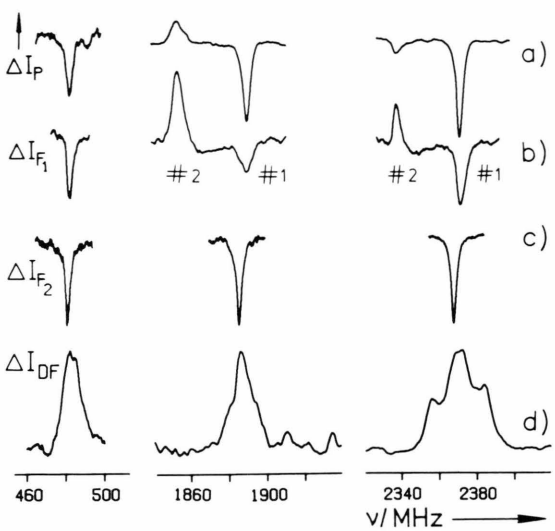

Fig. 1. The ODMR spectrum of A/TCPA at 1.2 K: a) excitation above or below the S_1 band, detection on phosphorescence (p-ODMR), b) excitation below the S_1 origin, detection on fluorescence (F_1-ODMR), c) excitation above the S_1 origin, detection on fluorescence (F_2-ODMR), d) excitation above the S_1 band or into one of the T_1 bands, detection on delayed fluorescence (DF-ODMR).

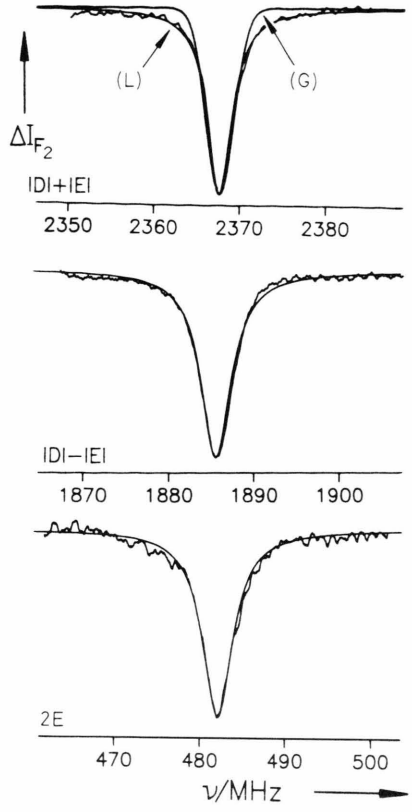

Fig. 2. The zero-field F_2-ODMR transition at 1.2 K (optical excitation above the S_1 band). Also drawn are Lorentz curves of the corresponding width as well as a Gauss curve (G) for the $|D|+|E|$ transition.

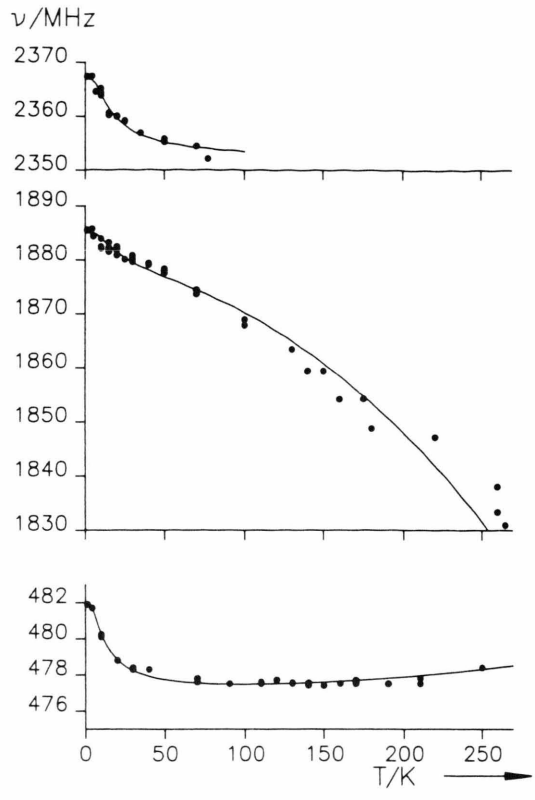

Fig. 3. The temperature changes of the F_2-ODMR transition frequencies. The lines were simulated using the parameters from Table 1 and assuming the two responsible mechanisms discussed in 4.1.2.

which made it possible to establish their shape (Fig. 2) as Lorentzian. The zfs parameters are:

$$|D| = 2126.5(3), \quad |E| = 241.0(3)\ \text{MHz}.$$

They do not change between 1.2 and 4.2 K. The linewidth is 4.3 MHz for the $2|E|$ and $|D|-|E|$ transitions and 3.4 MHz for the $|D|+|E|$ one at high rf-power level. These values converge to the following homogeneous linewidths with decreasing rf-power:

$$2|E|: \quad \Delta\nu_{1/2} = 2.3 \pm 0.2\ \text{MHz},$$
$$|D|-|E|: \quad \Delta\nu_{1/2} = 2.0 \pm 0.2\ \text{MHz},$$
$$|D|+|E|: \quad \Delta\nu_{1/2} = 1.8 \pm 0.2\ \text{MHz}.$$

The $2|E|$ and $|D|-|E|$ F_2-ODMR signals could be followed up to room temperature, the $|D|+|E|$ signal only to 70 K. The $2|E|$ frequency exhibits only a very small shift, but the two other frequencies decrease significantly with increasing temperature (Figure 3). This means that the D value stronlgy depends on temperature while the E parameter is only weakly temperature-dependent. A curious fact is a 1 MHz hysteresis of the $2|E|$ transition frequency between 70 and 180 K between the cooling and warming cycle. This may be a hint to further changes of the crystal structure at lower temperatures.

The F_1-ODMR spectra from Fig. 1, repeated with high resolution, exciting below the S_1 band, are shown in Figure 4. The signals are asymmetrical and partially structured, but the individual components could not be fully resolved. The zfs parameters derived from the maxima of the signals are

$$|D| = 2128.7(2), \quad |E| = 240.9(2)\ \text{MHz}.$$

The signal amplitude reaches maximum at lower rf-power levels (10 mWatt) than the F_2-ODMR lines. Within the F_1-ODMR signals the individual compo-

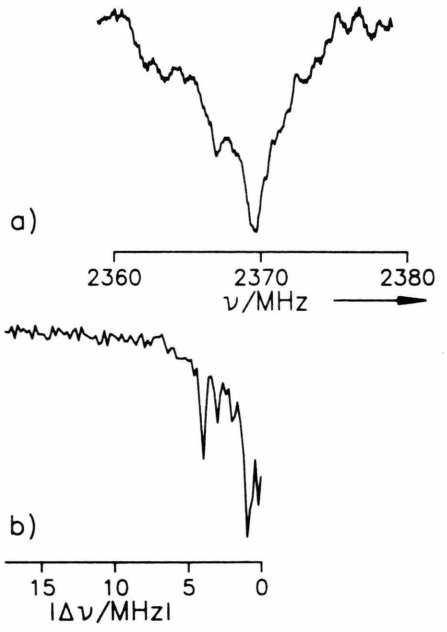

Fig. 4. a) The $|D|+|E|$ F_1-ODMR signal (optical excitation below the S_1 band with improved resolution at 1.2 K and b) a Fourier transform of the electron spin echo shown in Figure 6.

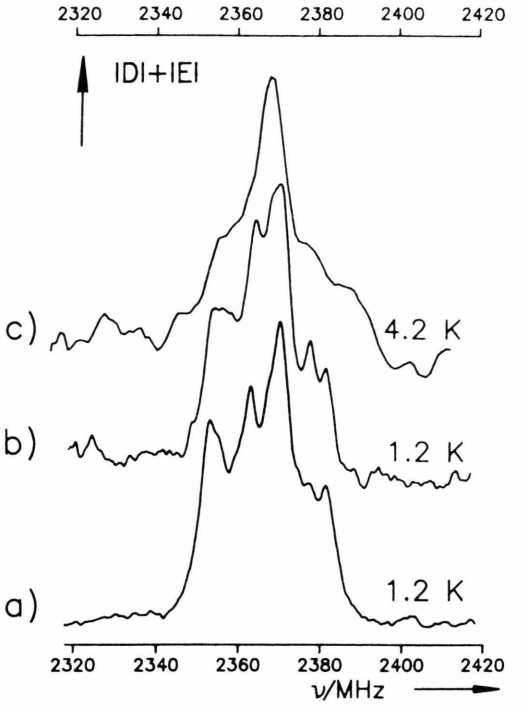

Fig. 5. The $|D|+|E|$ DF-ODMR transition at different temperatures and microwave powers: 1.5 Watt (a), 4 Watt (b) and 2 Watt (c).

nents saturate differently. The F_1-ODMR signals could be followed with excitation wavelengths up to 514.5 nm and in the temperature range from 1.2 to 3.4 K.

3.1.2. DF-ODMR

The DF-ODMR experiments were performed between 1.2 and 4.2 K. The delayed fluorescence was induced either by directly populating the T_1 state with the dye laser, or via the S_1 state. The signals are remarkably broad and structured (Figure 5). This structure is reproducible in all the samples examined, independently of the growth conditions and method, and therefore can be assigned to intrinsic defects present in the crystals. In fact, careful examination of the partially resolved structure allows to identify at least 4 distinct states with slightly different zfs parameters.

The broad DF-ODMR signals can be detected also while exciting the crystal below the S_1 band, e.g. with the 448 nm laser line, but with a strongly reduced intensity.

The signals undergo profound changes with increasing temperature (Figure 5). At 4.2 K one DF-ODMR line dominates in a given transition at exactly the same frequency and characterized by the same linewidth as the corresponding F_2-ODMR signal in Figure 1.

3.2. Pulsed ODMR

Pulsed ODMR experiments were performed by two different methods. The first one corresponds to the procedure of van Dorp et al. [10] and will be subsequently called "short-pulse" method. It depends on a short perturbation of the system by a δ-like microwave pulse, whereby the pulse length must be short relative to the intrinsic constants of the triplet state.

The second method was that of Clarke et al. [11]. It depends on a long, saturating microwave pulse. One observes the changes of optical emission on switching the rf power on and off. It will be called a "long-pulse" method.

Details about both methods can be found in [10, 11]. In our experiments both of them were conducted under continuous optical excitation conditions. Only results relevant for the discussion will be presented

below. It is necessary to mention that, although both procedures were originally developed for F-ODMR, they can also be employed in DF-ODMR taking into consideration the triplet-triplet annihilation rate.

3.2.1. Pulsed F-ODMR

The pulsed F-ODMR experiments were performed with excitation above the S_1 origin. The "short-pulse" procedure yields a biexponential response which can be resolved into two components (we neglect a very fast component of the order of nanoseconds, which could not be resolved):

$$\tau_1 \cong 25\ \mu s \triangleq k_1 = 4.1(1) \times 10^4\ s^{-1},$$
$$\tau_2 \cong 180\ \mu s \triangleq k_2 = 5.5(6) \times 10^3\ s^{-1},$$

with the amplitude ratio of $A_1/A_2 = 10$. As the applied light intensity was high (100 mWatt) in order to secure a proper detection, these k-values are artificially increased.

For a better characterization of the stronger component we performed the experiments according to the "long-pulse" method, applying 20–50 μs pulses. The reaction of the system to switching the rf power on and off is shown in Figure 6. The very fast optical response to the microwaves is again below instrumental resolution (0.5 μs). The return to equilibrium after switching off the rf power yields the same time constant τ_1 as from the short-pulse experiment. This experiment could be conducted with decreased light intensity, and the following values were found for the three transitions by extrapolating to zero light intensity:

$$\tau_1^{xz} = 62 \pm 8\ \mu s \triangleq k_1^{xz} = (1.6 \pm 0.2) \times 10^4\ s^{-1},$$
$$\tau_1^{yz} = 50 \pm 10\ \mu s \triangleq k_1^{yz} = (2.0 \pm 0.5) \times 10^4\ s^{-1},$$
$$\tau_1^{xy} = 90 \pm 20\ \mu s \triangleq k_1^{xy} = (1.1 \pm 0.3) \times 10^4\ s^{-1}.$$

3.2.2. Pulsed DF-ODMR

The pulsed DF-ODMR experiments were performed on the $|D|-|E|$ and $|D|+|E|$ transitions. As these transitions had been proved to have a complex nature, the pulse experiments were carried out at different frequencies within the broad signals.

It was found that the delayed fluorescence reacts to the long rf pulse with two constants: one shorter than the resolution time (in this case 5 μs), the other one of about 1 ms. The same response times can be found in the return to the initial state after switching off the microwaves. The long response times are

$$\tau = 0.45 \pm 0.05\ ms \quad (1890\ MHz, |D|-|E|),$$
$$\tau = 0.60 \pm 0.09\ ms \quad (2365\ MHz, |D|+|E|).$$

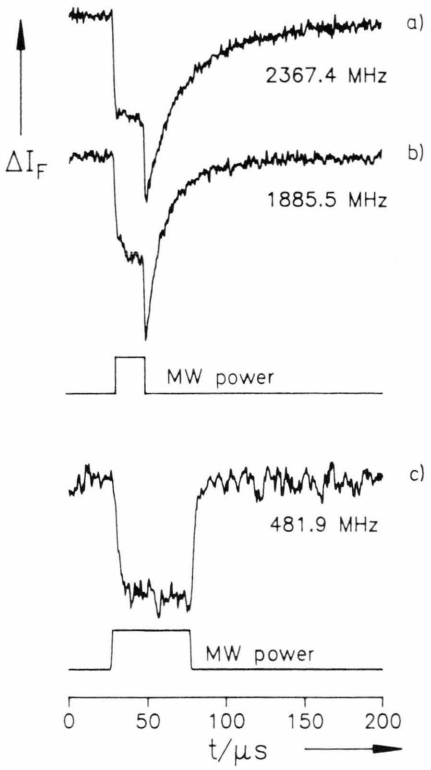

Fig. 6. The time response of the fluorescence to microwave pulses at excitonic frequencies (conditions analogous to the cw-F_2-ODMR experiment of Figure 2). Number of accumulations necessary to obtain the shown $|D|+|E|$ response: 145,000.

The shorter response times were obtained via the short pulse method for the $|D|-|E|$ and $|D|+|E|$ transitions at different rf frequencies in this range. For clarity the results are presented here for two frequencies only: one representing the value at which the characteristic "F_1-ODMR" signal appears in DF at 4.2 K (see Fig. 5), the other shifted a few MHz, corresponding roughly to the maximum of the very asymmetrical DF-ODMR signal. An example of such a measurement is shown in Figure 7. The response is biexponential and frequency-dependent.

For the $|D|-|E|$ transition the resolved response times are

$$\tau_1 = 1.4 \pm 0.2\ \mu s, \quad \tau_2 = 13.4 \pm 1.4\ \mu s \text{ at } 2367.4\ MHz^*,$$
$$\tau_1 = 1.6 \pm 0.2\ \mu s, \quad \tau_2 = 7.3 \pm 1.5\ \mu s \text{ at } 2365.0\ MHz.$$

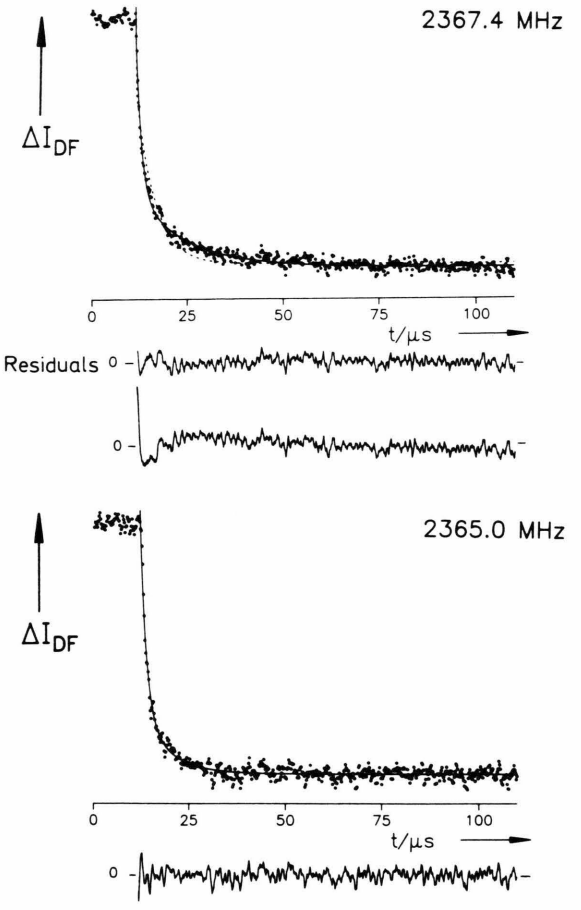

Fig. 7. The time response of delayed fluorescence to switching off the microwaces of the frequency within the broad $|D|+|E|$ DF-ODMR transition shown in Figure 5. The lines were drawn using the parameters from the text (3.2.2.).

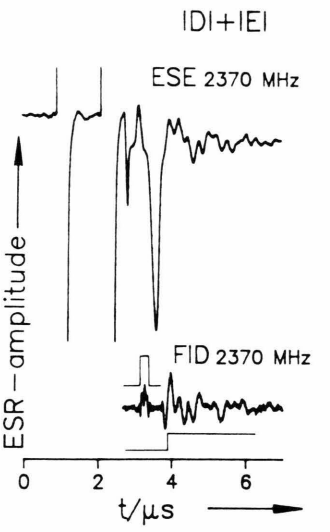

Fig. 8. Microwave-detected electron spin echo (ESE) and free induction decay (FID) under conditions optimal for F_1-ODMR experiment ($T = 1.2$ K, excitation under the S_1 band). Also shown is the microwave excitation pulse for the FID and the detection gate opening.

For the $|D|+|E|$ transition the times are

$\tau_1 = 1.6 \pm 0.3$ μs, $\tau_2 = 15.8 \pm 2.8$ μs at 1885.5 MHz*,

$\tau_1 = 2.0 \pm 0.5$ μs, $\tau_2 = 17.0 \pm 3.0$ μs at 1890.0 MHz.

Note that the longer response time τ_2 is frequency dependent, while τ_1 is not.

3.3. Pulsed ESR in Zero Field

The microwave-detected pulsed ESR experiments were carried out under two essentially different conditions: with excitation below and above the S_1 origin. Recalling Fig. 1, these are the conditions under which the F_1-ODMR signals and the F_2-ODMR signals, respectively, dominate in the cw-F-ODMR spectrum.

The detection of the two-pulse Hahn-echo ($\pi/2 - \tau - \pi$) [6] as well as the FID (free induction decay) was possible. Figure 8 shows the results obtained for two transitions with the optical excitation below the S_1 band. In both cases the echo form is complex, revealing an overlap of various oscillations. The same phenomenon is visible in the FID, with the maxima and minima of the oscillations corresponding to the shape of the echo.

The echo intensity as a function of the interval τ between the pulses is shown in Fig. 9 for two ODMR transitions. For $2\tau > 3$ μs the decrease of the echo amplitude is monoexponential with a characteristic decay time (transverse relaxation time) $T_2 = 3.6(1)$ μs. Substituting this value in the well-known formula

$$\Delta\nu_{1/2}^{\text{hom}} = (\pi T_2)^{-1}, \tag{1}$$

we derive the half-width of the homogeneous line

$$\Delta\nu_{1/2}^{\text{hom}} = 0.09 \text{ MHz}.$$

As mentioned above, pulsed ESR experiments were carried out also under conditions typical for obtaining the optimal F_2-ODMR spectra, i.e. excitation above

* Anticipating the discussion, F_1-ODMR signals at these frequencies are attributed to mobile triplet excitons.

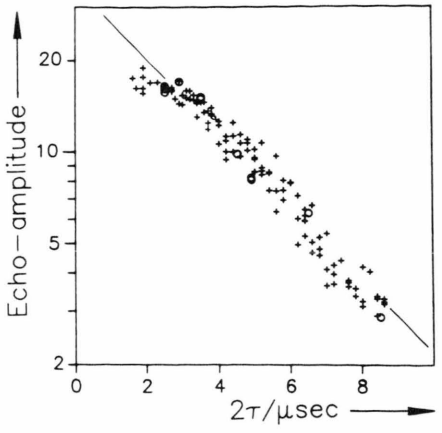

Fig. 9. The intensity of ESE from Fig. 8 as a function of time delay between the two pulses at the $|D|-|E|$ (crosses), and the $|D|+|E|$ transition frequency (circles). The line was drawn using the transverse relaxation time 3.6 μs.

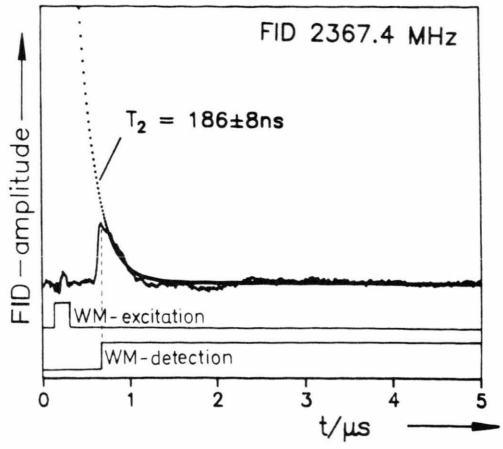

Fig 10. Microwave-detected FID of the excitonic (F_2-ODMR) signal at 1.2 K. The line was drawn with the transverse relaxation time 186 ns.

the S_1 origin. The most significant result in this case was the failure to detect the spin echo, even after most careful adjustment of the pulse lengths and averaging of over 500,000 responses. According to theory, the echo should not appear for homogeneous lines, therefore the lack of an echo can be considered as a proof of the homogeneity of the F_2-ODMR signals. We concentrated therefore on measuring the FID. It was not an easy task, as because of the relatively large value of the homogeneous linewidth (~ 2 MHz, see 3.1.1.) the decay time of the FID is very short and most of the signal amplitude is lost within the resolution time. However, the signal was recorded with the excitation wavelengths of 457.9 and 476.5 nm (above the S_1 band) (Fig. 10) but could not be detected with the excitation wavelength of 488.0 nm. The measured decay time of the FID of the $|D|+|E|$ transition is 186 ± 9 ns, which according to (1) yields the homogeneous linewidth of 1.7 MHz, in excellent agreement with the results of the cw-F-ODMR.

3.4. Cw-ESR in High Field

Standard high-field ESR experiments revealed the presence of one pair of characteristic triplet signals in the whole temperature range accessible (3.8–295 K). They could be detected with excitation into and below the S_1 band, but the excitation conditions affected the spin polarization pattern of the spectrum. The linewidth is orientation-dependent and is 1.5 G for $B \parallel y$, 2.0 G for $B \parallel z$ and 2.8 G for $B \parallel x$ at 295 K (x = long in-plane, y = short in-plane and z = out-of-plane axis of anthracene). It decreases very slightly upon cooling the crystal down to 100 K and increases again below this temperature. The values at 3.8 K are 1.7, 2.9 and 3.8 G, respectively. The signals do not saturate easily even at low temperature.

The zfs parameters obtained from the rotation patterns of the ESR signals agree well with the parameters obtained from the F_2-ODMR spectra at the same temperature. Most important, the temperature behavior of the D value is exactly the same as the one obtained from the ODMR spectra. The variations of the E parameter are too small to be detected by ESR.

On lowering the temperature to about 4.2 K a pair of new signals appears in the ESR spectrum at exactly the same magnetic field positions as the high-temperature signals. Their intensity is much higher with below-the-band excitation, when they almost completely mask the previously described lines (Figure 11). Their most characteristic feature is a neatly resolved hyperfine structure at B approximately $\parallel x$. Careful examination of the hfs pattern show that we have to do with two sets of anthracene hfs structure [12] differing in orientation by 1–2 degrees. Following the angular dependence of the individual sets was not possible, as the hfs structure merges into one broad line outside the very narrow angular region corresponding to $B \parallel x \pm 2$ deg. The individual hfs lines are split by 4.25 G. The high-temperature signals, however, can still be detected even at 3.8 K, particularly at a high microwave power, when the others easily saturate, or

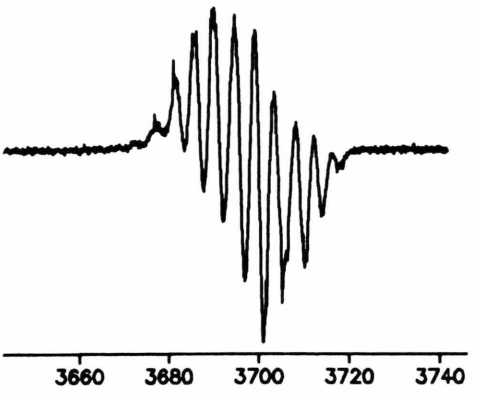

Fig. 11. The high-field ESR signal of a deep triplet trap at 3.8 K and magnetic field parallel to the high-temperature phase anthracene x axis. The hfs structure originates from anthracene in two slightly different orientations. Optical excitation below the S_1 band.

under excitation above the S_1 origin, when their amplitude is much higher in relation to the structured signals.

4. Discussion

4.1. Triplet Excitons

4.1.1. Singlet-Triplet Energy Transfer and CT Character

In the earlier paper [3] it was claimed that the F_2-ODMR signals observed under excitation into the S_1 band are due to mobile triplet excitons, even at the lowest obtainable temperature of 1.2 K. However, the decisive proofs were missing until now, when we were able to determine accurately the shape of the signals (Lorentzian for all the transitions) as well as their homogeneous character (the lack of a spin echo). This assertion is further corroborated by the ESR experiments. In the ESR spectrum it was possible to follow the excitonic signals, which had been earlier identified as such [4] down to the lowest attainable temperature of 3.8 K. Up to our knowledge it is a unique observation in a CT crystal, as usually the excitonic signals in these systems are either masked at low temperature by ever-present traps, or the excitons become immobilized by self-trapping [5].

Very interesting is the observation of the presence of excitonic ESR signals while exciting the crystal deep below the S_1 band, that is into one of the singlet traps. In fact, the intensity of these signals does not decrease even when the excitation wavelength is 514 nm. This is in agreement with the optical results [1], where under the same excitation conditions delayed fluorescence was found. The ESR brings an additional suggestion, that in the excitation path from the S_1 trap to the T_1 band there must be an intermediate triplet state, as the spin-polarization pattern is different at low-energy excitation as compared to excitation above the S_1 origin.

In order to estimate the CT character of the triplet excitons we can use the standard formula [13] based on the determination of the fine structure parameters and the comparison with the zfs of the local triplet state:

$$c_{\mathrm{CT}}^2 = \frac{D^{\mathrm{loc}} - D^{\mathrm{exp}}}{D^{\mathrm{loc}} - D^{\mathrm{ion}}}, \tag{2}$$

where

D^{loc}: the D parameter of the neutrally excited triplet state of the acceptor or the donor,

D^{exp}: the experimental determined D parameter of the complex,

D^{ion}: the D value of the ionic (charge-transfer) form (D^+A^-).

(The parameter E may also be used in the estimation.)

The T_1 state of TCPA can be ignored in the calculations, having a much higher energy than anthracene (23 700 cm^{-1} [14]). As D_{loc} and E_{loc} the corresponding values of anthracene should be taken, but this poses a serious problem. A review of the literature data on the T_1 state of anthracene shows large variations of zfs parameters depending on the environment of the molecules. Excitons in pure anthracene crystal should not be used for comparison, as they have smaller zfs parameters than the traps in A/TCPA. It seems that the best reference values are those of an isolated anthracene molecule in an inert matrix. We took therefore the values in an n-heptane glass [15]:

$$|D| = 2186.5 \text{ MHz}, \quad |E| = 245.5 \text{ MHz}.$$

Substituting them into (2) we obtain

$c_{\mathrm{CT}}^2 = 3\%$ (4%) from the lowering of the $D(E)$ value.

The CT character of the triplet excitons has recently been estimated by an independent optical method of following the temperature dependence of the zero-phonon line intensity in the triplet excitation spectrum, thus determining the exciton-phonon coupling constant [16]. The result of this experiment ($c_{\mathrm{CT}}^2 = 8\%$) is in reasonable agreement with our value.

4.1.2. Temperature Dependence of the Fine Structure

The temperature dependence of the zfs parameters in A/TCPA can be analyzed in terms of two different contributions, see Figure 3. This classification can be easily understood if we assume that the process activated at high temperature converges to zero at low temperature, and vice versa. At any temperature the two processes are superimposed, so we may write

$$D(T)=D_{\mathrm{L}}(T)+D_{\mathrm{H}}(T), \quad (3)$$

(L = low, H = high temperature).

In the following we attempt to ascribe

- $D_{\mathrm{L}}(T)$ to the exciton hopping between the two triplet bands T_{A} and T_{B}, whose existence is known from the excitation spectroscopy (the dominant process at $T<100$ K),
- $D_{\mathrm{H}}(T)$ to the librations of anthracene molecules known to take place from the X-ray analysis [1] (the process dominant at $T>100$ K).

Both processes lead to an averaging of the zfs tensors.

A) Temperature $T<100$ K

In this temperature range there are two inequivalent sublattices in the crystal [1]. To each of them an individual triplet band is attributed, each in turn characterized by a zfs tensor. The two tensors are expected to differ not only in orientation relative to the crystal axes, but also in the zfs parameters (i.e. D_{A}, $E_{\mathrm{A}} \neq D_{\mathrm{B}}$, E_{B}). Even with D_{A}, $E_{\mathrm{A}} \equiv B_{\mathrm{B}}$, E_{B} one should expect an ESR spectrum of two separated pairs of signals. The minimal value of this splitting can be estimated from the cystal structure taking into account the orientation differences

$\Delta B = 6$, 1.5, and 7.5 G for $B \parallel x$, y, and z, respectively.

With a calculated Boltzmann population of the two bands of 60:40 at 100 K and the linewidth of max. 2.2 G, both sets of signals should be readily observable. Careful measurements, however, of the ESR spectra of many crystals in multiple orientations yielded always only one pair of excitonic lines. Consequently, it is necessary to assume that the excitons in their movement through the crystal are scattered between the two triplet bands with a frequency higher than the frequency difference of their magnetic resonance signals, i.e. min. 7.5 G $\cong 2\times10^{7}\ \mathrm{s}^{-1}$. Such a scattering averages the zfs tensors of the two sublattices present in the low-temperature phase, so that only a mean zfs tensor is measured at a given temperature.

Besides the averaging, the interband hopping results in a temperature dependence of zfs parameters, as the hopping is thermally activated (see 4.1.3.). This is exactly what was found experimentally both in zero field (F_2-ODMR) and in high field (ESR). A temperature dependence of the fine structure has been previously found in most of CT crystals [17], but what makes A/TCPA unique is that this dependence starts at very low temperature (practically already at 4.2 K). In order to analyze quantitatively this process, the following model was developed, based on the "jumping spin" theory [18].

In the case of a fast exciton exchange between two magnetically inequivalent sites "A" and "B" having the Larmor frequencies ω_{A} and ω_{B} there appears in the ESR spectrum a single line centered on the frequency

$$\bar{\omega}=f_{\mathrm{A}}\,\omega_{\mathrm{B}}+f_{\mathrm{B}}\,\omega_{\mathrm{B}}\,, \quad (4)$$

where

$$f_{\mathrm{A}}=\frac{P_{\mathrm{BA}}}{P_{\mathrm{AB}}+P_{\mathrm{BA}}} \quad \text{and} \quad f_{\mathrm{B}}=\frac{P_{\mathrm{AB}}}{P_{\mathrm{AB}}+P_{\mathrm{BA}}} \quad (f_{A}+f_{\mathrm{B}}=1).$$

P_{AB} and P_{BA} are the probabilities of the jumps "A"→"B" and "B"→"A", f_{A} and f_{B} are therefore the probabilities of populating the levels "A" and "B", respectively.

If the two sites are in thermal equilibrium, that is if $P_{\mathrm{AB}}/P_{\mathrm{BA}}=\exp(-\varepsilon/kT)$, where ε is the energy difference of the sites, the observed frequency of the signal ν_{ODMR} is also thermally activated, and so are the zfs parameters $\bar{D}$ and $\bar{E}$ [19]:

$$\bar{D}=D_{\mathrm{A}}+(D_{\mathrm{B}}-D_{A})\frac{\exp(-\varepsilon/kT)}{1+\exp(-\varepsilon/kT)} \quad (5\mathrm{a})$$

and

$$\bar{E}=E_{\mathrm{A}}+(E_{\mathrm{B}}-E_{\mathrm{A}})\frac{\exp(-\varepsilon/kT)}{1+\exp(-\varepsilon/kT)}\,, \quad (5\mathrm{b})$$

where D_{A}, E_{A} and D_{B}, E_{B} are the zfs parameters of the lower and higher states. The highest expected shifts of D and E are

$$\bar{D}(\infty)-\bar{D}(0)=(D_{\mathrm{B}}-D_{\mathrm{A}})/2\,, \quad (6\mathrm{a})$$

$$\bar{E}(\infty)-\bar{E}(0)=(E_{\mathrm{B}}-E_{\mathrm{A}})/2\,. \quad (6\mathrm{b})$$

The above equations are valid if the two tensors have different zfs parameters but the same orientation. In case of an orientation difference we have to calculate the eigenvalues of an averaged tensor:

$$\mathbf{F} = f_A \cdot \mathbf{F}_A + (1 - f_A) \cdot \mathbf{F}_B$$

$$= \frac{1}{1+\exp(-\varepsilon/kT)} \cdot \mathbf{F}_A + \frac{\exp(-\varepsilon/kT)}{1+\exp(-\varepsilon/kT)} \cdot \mathbf{F}_B, \quad (7)$$

when $P_{AB}/P_{BA} = \exp(-\varepsilon/kT)$.

The tensor $\mathbf{F}_B$ of the higher-lying state may be expressed in terms of the tensor $\mathbf{F}_A$ and the orientation difference between them in a perturbation consideration:

$$\mathbf{F}_B = \boldsymbol{T}^{-1} \begin{pmatrix} X^* & & \\ & Y^* & \\ & & Z^* \end{pmatrix} \boldsymbol{T}, \quad (8)$$

where $X^* = (D_A + \delta D)/3 - (E_A + \delta E)$,
$Y^* = (D_A + \delta D)/3 + (E_A + \delta E)$,
$Z^* = 2/3(D_A + \delta D)$,

and $\boldsymbol{T}$ is the orthonormalized transformation matrix describing the orientation difference of the two tensors.

The experimental data used in the fitting procedure were the following: $D_A = 2126.5$ MHz, $E_A = 241.0$ MHz (these are the excitonic zfs values at 1.2 K), $\varepsilon = 40\ \mathrm{cm}^{-1}$ (from the optical spectra), and

$$\boldsymbol{T} = \begin{pmatrix} .997895 & .0348879 & .0540799 \\ -.0321074 & .998185 & -.0509283 \\ -.0579481 & .0490709 & .997112 \end{pmatrix}$$

(from the crystal structure).

The diagonalization of (7) causes the simple analytical form of $\bar{D}(T)$ and $\bar{E}(T)$ to get lost. However, we found that the temperature dependence of $\bar{D}$ (and $\bar{E}$) can still be expressed analytically with an insignificant error by a linearization similar to (5):

$$\bar{D}(T) = D_A + 2\Delta D^* \frac{\exp(-\varepsilon^*/kT)}{1+\exp(-\varepsilon^*/kT)}, \quad (9)$$

where ε^* is an "effective" activation energy obtained via a simulation calculation using the experimental points. It is equal to $33\ \mathrm{cm}^{-1}$ (rather than $40\ \mathrm{cm}^{-1}$), and $2\Delta D^* = \bar{D}^*(\infty) - \bar{D}^*(0\ \mathrm{K})$ is greater then $D_B - D_A$. This iteration procedure was finally used to fit the δD and δE values to the experimental data. Actually, the experimental points were the ODMR frequencies, so instead of fitting the ΔD^* value, we fitted the corresponding "effective" ODMR frequencies Δ_{ij} $(i, j = x, y, z)$:

$$\nu_{ij}(T) = \nu_{ij}^0 + 2\Delta_{ij}^{\nu} \frac{\exp(-\varepsilon^*/kT)}{1+\exp(-\varepsilon^*/kT)}. \quad (10)$$

The results of the numerical fits are as follows:

from the $|D|+|E|$ transition:

$$\Delta_{xz} = 15 \pm 2\ \mathrm{MHz}, \qquad \varepsilon_{xy}^* = 16 \pm 3\ \mathrm{cm}^{-1};$$

from the $|D|-|E|$ transition:

$$\Delta_{yz} = -9 \pm 1\ \mathrm{MHz}, \qquad \varepsilon_{yz}^* = 21 \pm 6\ \mathrm{cm}^{-1};$$

from the $2|E|$ transition:

$$\Delta_{xy} = -4.5 \pm 1\ \mathrm{MHz}, \qquad \varepsilon_{xy}^* = 12 \pm 4\ \mathrm{cm}^{-1}.$$

From these we obtain

$$\Delta D^* = (\Delta_{xz} + \Delta_{yz})/2 = -12 \pm 1\ \mathrm{MHz},$$
$$\Delta E^* = \Delta_{xy}/2 \qquad = -2.2 \pm 0.5\ \mathrm{MHz}.$$

We can now calculate the difference between the zfs parameters of the tensors $\mathbf{F}_A$ and $\mathbf{F}_B$ using (8) and (9):

$$\delta D (= |D_B| - |D_A|) = -14\ \mathrm{MHz},$$
$$\delta E (= |E_B| - |E_A|) = -\ 3\ \mathrm{MHz}.$$

The results of the fits are also presented in Fig. 3 in terms of the simulated temperature dependencies of zfs frequencies. In Table 1 the zfs parameters and the ODMR frequencies of the two triplet tensors are listed. The "effective" activation energies obtained from the calculations are lower than the value of $33\ \mathrm{cm}^{-1}$ expected from the model (see above). The reason of this discrepancy may be the fact that the model presented above is valid for $T < 100$ K while the orientation matrix $\boldsymbol{T}$ is based on the crystal structure determined at 120 K. It is highly probable that the mutual orientation of the anthracene molecules at $T < 100$ K are different from those at 120 K, and this could lead to the difference in the calculations.

From a similar procedure applied to the high-field ESR spectra we obtained very similar values for D (the

Table 1. Zfs parameters and ODMR frequencies of the two fine structure tensors originating from the two triplet bands T_A and T_B.

$D_A = 2126.5$ MHz	$D_B = 2112.5$ MHz
$\lvert E_B \rvert = 241.0$ MHz	$\lvert E_B \rvert = 238.0$ MHz
$\nu_A^{xz} = 2367.4\ MHz$	$\nu_B^{xz} = 2350.4$ MHz
$\nu_A^{yz} = 1885.5$ MHz	$\nu_B^{yz} = 1874.5$ MHz
$\nu_A^{xy} = 481.9$ MHz	$\nu_B^{xy} = 475.9$ MHz

poorer accuracy of the high-field method did not allow to determine the temperature dependence of E):

$$\Delta D^* = -14.5 \pm 3 \text{ MHz}, \quad \varepsilon^* = 30 \pm 10 \text{ cm}^{-1}.$$

Also, it was found by the calculations that the fine structure principal axes of the averaged (i.e. experimentally determined) tensor should change their positions by only 1.5 deg. between 4 and 120 K. Such small shifts, if present, lie within the experimental error of the ESR and were not detected.

B) Temperature $T > 100$ K

At $T > 100$ K we assume the dominating mechanism responsible for the temperature dependence of the zfs parameters to be seen in librations of the molecules, as analogously in other CT crystals, e.g. N/TCNB [20] or A/TCNB [17]. However, in N/TCNB, in which the triplet excitons have a 25% CT character, such librations lead to a decrease of the CT character and consequently to an increase of the zfs parameters. In A/TCPA, the D value decreases in the whole temperature range. Therefore we assume that these changes are caused by an averaging of the two zfs tensors described in the previous section through molecular librations, in analogy with A/TCNB in [17].

The averaged zfs tensor $\mathbf{F}_{\text{lib}}$ can be represented by

$$\mathbf{F}_{\text{lib}} = [\mathbf{F}(-\alpha) + \mathbf{F}(+\alpha)]/2$$

for a libration about the x axis (α is the angular amplitude of this libration), and similarly for librations about the other two symmetry axes. For small amplitudes of the librations they may be treated independently from each other. We have found by numerical calculations that the temperature dependence of the zfs parameters in the high-temperature regime can be described by the following expressions:

$$\bar{D} = D_0 - 0.2156\,\alpha^2 - 0.2700\,\beta^2,$$
$$2|\bar{E}| = 2E_0 + 0.1438\,\alpha^2 - 0.1800\,\beta^2 - 0.073\,\gamma^2$$

with $D_0 = 2114$ MHz and $2|E_0| = 478$ MHz (obtained from the corresponding zfs values of the excitons at 1.2 K reduced by the thermally activated contribution calculated with (9)), and α, β, γ = libration amplitudes about the x, y, z symmetry axes. As we have here three variables but only two equations, it is not possible to calculate the libration amplitudes at a given temperature. However, from the increase of $|E|$ observed experimentally we also have: $\alpha^2 > 1.25\,\beta^2 + 0.51\,\gamma^2$. If we assume $\alpha/\beta = 1.5$ we have then at 290 K

$$\alpha = 5.5, \quad \beta = 3.5, \quad \gamma = 4.5°.$$

The relation $\alpha > \gamma > \beta$ agrees very well with the structural data [1] at 230 K:

$\alpha = 4.4$, $\beta = 2.9$, $\gamma = 3.4°$ for the A_1 molecule,

$\alpha = 3.8$, $\beta = 2.2$, $\gamma = 3.7°$ for the A_2 molecule.

If we extrapolate these data to 290 K, they are in good quantitative agreement.

4.1.3. Temperature Dependence of Excitonic Linewidth

The appearance of one pair of excitonic signals instead of the expected two, at least at low temperature, and the temperature dependence of fine structure are important clues to exciton dynamics. Another particularity of the A/TCPA crystal is the broadness of both zero-field and high-field transitions. Despite the significant linewidth, the Lorentzian shape of the ESR and ODMR signals in connection with the impossibility of obtaining a spin echo prove beyond reasonable doubt their homogeneous character. In such a case the linewidth is determined only by relaxation processes:

$$\Delta\nu_{1/2} = \frac{1}{\pi T_M} = \frac{1}{2\pi T_1} + \frac{1}{\pi T_2}, \tag{11}$$

where

T_M = the total dephasing time, consisting of
T_1 = spin-lattice relaxation time and
T_2 = spin-spin relaxation time.

T_2 consists further of multiple contributions:

$$\frac{1}{T_2} = \frac{1}{T_2^{\text{res}}} + \frac{1}{T_2^{\text{FS}}} + \frac{1}{T_2^{\text{HFS}}}, \tag{12}$$

where T_2^{res} = the residual spin-spin relaxation time, T_2^{FS} and T_2^{HFS} = exchange broadening due to fine and hyperfine interactions.

At high magnetic field the hyperfine interactions enter into the Hamiltonian in first order. If we assume that the observed ESR linewidths result from averaging of different hyperfine configurations, we can calculate the exciton hopping frequency P via the model of the "jumping spin" [18] by comparing the linewidths with those of the isolated triplet state of anthracene [21]. P is then given by the relation $P = \omega_i^2/\omega_{i\,\text{exp}}$. Table 2 summarizes the results of such estimations for

Table 2. ESR linewidths (in Gauss) of isolated anthracene triplet states and excitons in A/TCPA with the calculated exciton hopping rates (in s^{-1}).

Orientation	Anthracene [12, 34]	A/TCPA (excitons, 120 K) [this work]
$B \parallel x$	19 (1)	3.8 $P_x = 4.6 \times 10^8$
$B \parallel y$	8, 2 (0, 2)	1.7 $P_y = 1.8 \times 10^8$
$B \parallel z$	14 (1)	2.9 $P_z = 3.2 \times 10^8$

$T = 120$ K. The order of magnitude of the hopping frequency is consistent. The slightly different values point to an additional linewidth contribution of fine-structure averaging. This is even more pronounced at low temperature.

The decrease of the excitonic linewidth between 3.8 and 100 K may be due to a thermal activation of the exciton migration. This does not mean necessarily that the transfer integral is temperature-dependent. One may invoke in this place the concept of "caging barriers" [22], according to which the excitons at low temperature move inside "cages" created by defects. These "cages" can be overcome by thermal activation.

The narrowing process is not very efficient, though, as even at room temperature the ESR linewidth (> 1 G) remains at least one order of magnitude larger than the one recorded in other CT crystals (in the phenazine/TCNQ crystal a linewidth as small as 0.09 G was measured [23]), which may be explained by a relatively low hopping rate. The hopping rates listed in Table 2 are only total rates describing the jumps both within one sublattice and between the two sublattices. In order to estimate the latter (P_{AB} or P_{BA}) we use the value $P > 5 \times 10^7$ s^{-1} obtained from the conditions of appearing of one ESR signal instead of the expected two lines, taking into consideration also the orientation difference of the two zfs tensors (see 4.1.2.).

The slight increase of the ESR linewidth between 100 and 300 K may be tentatively attributed to thermally activated librations of the anthracene molecules.

If the observed large high-field linewidths can be assigned to the incomplete averaging of the hf structure complemented by the averaging of the fine structure, this explanation fails in the case of the zero-field signals, which are also relatively broad (1.8 to 2.3 MHz at 1.2 K and as much as 7 MHz at 77 K). This is so because the hyperfine interactions enter the zero-field Hamiltonian only in second order. For comparison, the inhomogeneous zero-field linewidth of isolated naphthalene is only 1.3 MHz [24]. The only plausible explanation seems to be hopping of the excitons betwen the two triplet bands. Its rate may be estimated from the conditions of the appearance of a single zf-ODMR line instead of two (their splitting can be calculated from the zfs parameters of the two tensors obtained in 4.1.2. and is shown in Table 1) as $P_{BA} > 4 \times 10^7$ s^{-1}, which is in good agreement with the high-field data.

The third important factor determining the excitonic linewidth is the spin-lattice relaxation (SLR) rate. It was measured by us in A/TCPA by a standard saturation technique [25] in zero field using a resonator. The scaling of B_{rf} had been done earlier by measuring the transient nutation of the phosphorescence of quinoline in deuterated naphthalene crystal as a function of the rf power. The measured SLR rate in A/TCPA is 2×10^4 s^{-1} at 1.2 K and 4×10^4 s^{-1} at 4.2 K.

The comparison of the SLR rate at 1.2 K with those obtained from pulsed DF-ODMR conducted at the excitonic frequencies ($1.1 - 2.0 \times 10^4$ s^{-1}, see 3.1.1.) shows a good correlation and allows to attribute the F-ODMR response constants measured for the three zero-field transitions to SLR rates.

The measured SLR rates are quite high in relation to the known values in other systems (e.g. for naphthalene in durene the rate is 10 s^{-1} at 2 K [26]). The reason for that may be seen again in the hopping of the excitons between the two triplet bands. A similar model was used to explain the SLR in anthracene in [27]. It was further developed in [28] to account for the SLR in the naphthalene/durene system. Without going into details, we found that employing this model for A/TCPA and using the previously determined zfs parameters of the two triplet bands we may explain the observed SLR rates if the interband hopping frequency P_{AB} between the bands at 1.2 K is $> 5 \times 10^6$ s^{-1}. This condition is certainly fulfilled in the A/TCPA crystal.

The SLR rates increase only very modestly with temperature, which is the principle reason for observing the zero-field ODMR signals even at 300 K.

4.2. Immobilized Triplet States

4.2.1. Deep Triplet Traps

The triplet traps present in the A/TCPA crystal and manifesting themselves in the phosphorescence spec-

trum have been previously rather arbitrarily divided into deep (depth $>40\,cm^{-1}$) and shallow (depth $<40\,cm^{-1}$) traps [3, 4]. This distinction was made because of the different ways these traps demonstrate themselves in the phosphorescence and ODMR spectra.

The number of different deep traps detected in the *phosphorescence* depends on the method the crystal was grown, and varies from 3 in sublimation-grown crystals to 7 in Bridgman-grown specimen. The depths of the individual traps are also dependent on the growth procedure, but are always within the energy range of $40-200\,cm^{-1}$. Contrary to this, the number of deep trap states discernible from the *ODMR spectra* is not dependent on the origin of the crystal, and is equal to two. They manifest themselves in the two distinct sets (#1 and #2) of the P-ODMR and F_1-ODMR signals (Figure 1). This might at first look like a discrepancy, but given the very small CT character of the triplet state in A/TCPA (see below), a slight misorientation of the donor molecule could alter the energy of the T_1 state without changing much the zfs parameters of the complex and hence the frequency of the ODMR transitions. The inhomogeneous linewidth of the F_1-ODMR signals and their asymmetry point to a greater number of trap states hidden under the common envelope. In fact, these "hidden" traps can be resolved by doing an Fourier transform of the spin echo (Figure 4). For example, in the transform of the $|D|+|E|$ signal there are two main peaks, recognizable also in the F_1-ODMR transition, together with three other weaker peaks.

The similarity of the zfs parameters of the two deep traps derived from the F_1-ODMR spectra with those of the excitons (see above) suggests strongly that their origin lies in structural faults of the crystal structure. Specifically, the zfs parameters of the trap #2 in the F_1-ODMR spectrum are so similar to those of the X-traps in the anthracene crystal [29] that an evident explanation seems to be a defect in the alternation order:

... ADADADD*DADADA ...
(A = acceptor, D = donor)

A/TCPA trap #2: $D = 2095$ MHz, $E = 241.5$ MHz,

anthracene [29]:

X-trap #1: $D = 2089$ MHz, $E = 237.7$ MHz,
X-trap #2: $D = 2081$ MHz, $E = 242.2$ MHz.

One of the deep traps responsible for the F_1-ODMR signals is visible also in the ESR spectrum at low temperatures. The well-resolved hyperfine structure of the ESR signals at 3.8 K is a typical feature of a trap state. We attribute these signals to one of the deep traps because they are best visible under the same conditions that are optimal for obtaining the F_1-ODMR spectrum (excitation at 488 nm, i.e. below the S_1 band). The hyperfine structure is often used in evaluation of the CT character alternatively to the fine structure [30]. However, if we compare the hyperfine splitting constant of the A/TCPA trap with the corresponding constants of anthracene in various environments, we encounter the same problem as with the fine structure parameters: these constants are often smaller than in A/TCPA. For example, for an anthracene trap in the biphenyl crystal the splitting constant is 4.0 G [12], while the one measured by us in A/TCPA is 4.25 G.

The fact that we have to do with two sets of zfs originating from anthracene in two slightly different orientations agrees very well with the structure of the low-temperature crystal phase [1]. It also confirms the above presented model of the hopping exciton and its influence on the fine structure: in the absence of the exciton movement we do indeed see the splitting of the ESR trap signals, which is not detected for excitons.

The deep traps #1 and #2 had their kinetic constants determined in [31]. The depopulation constants at 1.2 K are the following:

trap #1: $k_x = 37(5)$, $k_y = 33(5)$, $k_z = 9(3)\,s^{-1}$,
trap #2: $k_x = 50(5)$, $k_y = 32(5)$, $k_z = 8(3)\,s^{-1}$.

These results show very small differences relative to the X-traps in the anthracene crystal. Their relatively long lifetimes show that they are well isolated from the triplet band, i.e. there is no backward scattering into the band which would considerable shorten the lifetimes. This is also the reason for the very small homogeneous linewidth of the trap signals (90 kHz, see 3.3). The phase-relaxation time T_M measured by spin echo decay is 3.6 μs, which is comparable to other fully protonated aromatic molecules like tetrachlorobenzene in durene (3.2 μs, [32]). The only values measured for a CT crystal are those of A/TCNB, and they are also in good agreement (1.7 ... 3.3 μs, [33]).

4.2.2. Shallow Triplet Traps

The barely resolved structure of the DF-ODMR signals has to be attributed to trap states visible in the

DF via heterofusion processes. As this structure practically vanishes upon increasing the temperature from 1.2 to 2 K, these traps must be shallow. In fact, two of such immobilized states, 8 and 21 cm^{-1} deep, were previously found in the phosphorescence spectrum [3] at $T \leqq 2$ K.

The same pattern of shallow traps appears in all crystals examined, independent of their growth method. This means that these traps are intrinsic to the crystal. Their nature may be explainable by the low-temperature crystal structure of A/TCPA. Let us assume that instead of the regular, alternating pattern one of the asymmetrically shaped acceptor (TCPA) molecules is built in a "reversed" position. This leads immediately to four distinct possible configurations of this defect (Figure 12). As the CT character of the complex is very small, such defects involving a misorientation of TCPA should have only a small depth.

The kinetics of the shallow traps can be obtained from the pulsed DF-ODMR experiments. In comparison with the previously described [3] data derived from purely optical experiments with chopped light, the pulsed ODMR measurements give a better resolution time (50 ns vs. 50 μs) and the possibility of rf-frequency-dependent selectivity.

Contrary to the change of DF after switching the optical excitation off [3], which is in 30% "fast" ($\cong$μs, due to heterofusion) and 70% slow ($\cong$ms, due to homofusion), most of the DF reaction to switching the microwaves off is "fast", i.e. of the order of microseconds. The fastest reaction constant k_1 ($\tau_1 = 1.6$ μs), being equal for both $|D|-|E|$ and $|D|+|E|$ transitions and independent of the rf frequency, may be interpreted as the population rate of the T_1 state as a whole. The other constant, k_2, being frequency-dependent, may represent the rate of exciton capture by different traps.

The time response of the DF-ODMR signals to switching the microwaves on or off at the "excitonic" frequency is more complicated than the one of the traps. It suggests a strong interaction of the traps with the excitonic band, which requires further studies.

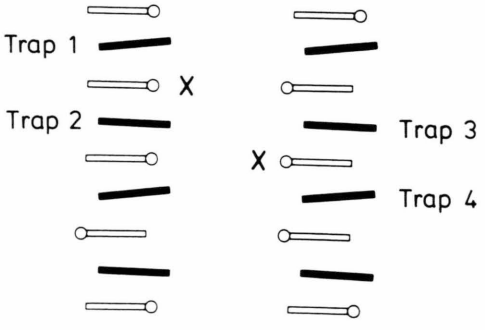

Fig. 12. A possible explanation of the shallow traps in A/TCPA. The TCPA molecule is shaped asymmetrically. (The circles represent the sides of oxygen.) A fault of the TCPA orientation (×) can point towards the anthracene planes (left) or off the planes (right). With two different anthracene orientations we end up with 4 different defect configurations.

5. Conclusions

Statements on the dimensionality of the triplet propagation are easily possible if there are differently oriented complexes in the unit cell, arranged separately in different, but neighbored stacks.

One of the best known example is Phenanthrene/PMDA in which the *inter*-stack hopping rates are at least two orders of magnitude smaller than the intra-stack ones. Separate triplet signals of both stacks are detectable therefore [35].

The situation in A/TCPA is more complicated because the complexes, inequivalent in symmetry (and zfs), are arranged alternatively *along* the stacking direction, and there are pairs of stacks in the unit cell.

Energy migration between non equivalent complexes can therefore be thought in stacking direction as well as orthogonal to it.

A dominant propagation in the latter direction, however, would connect equivalently oriented complexes with the consequence of two sets of excitonic signals at low temperatures. This is not observed!

Taking into account the stronger *inter*stack overlap of the anthracene orbitals within the pairs in each unit cell, the excitation must move preferentially in stacking direction visiting both stacks.

The exchange of the spins between different sites is reflected in the absolute values and the temperature dependence of frequencies and linewidths, which are explained with the jumping spin model.

This means a predominant *incoherent* hopping process with rates too slow for extreme narrowing.

The TCPA molecules, not included in the triplet excitation act just as "spacer" in order to "dilute" the anthracene system.

Acknowledgements

This work was supported by the Stiftung Volkswagenwerk (I/38427-Wo) and the Deutsche Forschungsgemeinschaft (POL 113/15). We would like to thank N. Karl and W. Tuffentsammer for growing the crystals and J. J. Stezowski and R.-D. Stigler for the discussions concerning the crystal structure.

[1] W. Mühle, J. U. von Schütz, H. C. Wolf, R.-D. Stigler, and J. J. Stezowski, to be published.
[2] G. Castro and R. M. Hochstrasser, J. Chem. Phys. **48,** 637 (1968).
[3] J. U. von Schütz, D. Burger, R. Krauss, W. Mühle, and H. C. Wolf, J. Luminesc. **24/25,** 467 (1981).
[4] B. Kozankiewicz, J. Prochorow, and J. Krzystek, Mol. Cryst. Liq. Cryst. **75,** 17 (1981).
[5] W. Mühle, J. Krzystek, J. U. von Schütz, H. C. Wolf, R.-D. Stigler, and J. J. Stezowski, Chem. Phys. **108,** 1 (1986).
[6] J. H. van der Waals, in: Time Domain Electron Spin Resonance (L. Kevan and R. L. Schwartz, eds.), Wiley, New York 1979, p. 343.
[7] T. Moreno, Microwave Transmission Design Data, Dover Publications, New York 1949.
[8] W. Mühle, Ph.D. Thesis, Universität Stuttgart 1987.
[9] W. Höptner and J. U. von Schütz, unpublished.
[10] W. G. van Dorp, W. H. Shoemaker, M. Soma, and J. H. van der Waals, Mol. Phys. **30,** 1701 (1975).
[11] R. H. Clarke, in: Triplet State ODMR Spectroscopy (R. H. Clarke, ed.), Wiley, New York 1982.
[12] J.-Ph. Grivet, Chem. Phys. Letters **4,** 104 (1969).
[13] H. Möhwald and E. Sackmann, Z. Naturforsch. **29a,** 1216 (1973).
[14] M. Sano, T. Narisawa, N. Matsuka, and J. I. Haya, Bull. Chem. Soc. Japan **50,** 2266 (1979).
[15] R. H. Clarke and J. M. Hayes, Chem. Phys. Letters **27,** 556 (1974).
[16] S. Maier and H. Port, Z. Naturforsch. **42a,** 1261 (1987).
[17] J. U. von Schütz, J. Krzystek, W. Mühle, R. Sauter, and H. C. Wolf, Abstracts of the 11th Molecular Crystal Symposium, Lugano 1985, p. 301.
[18] A. Carrington and A. D. McLachlan, Introduction to Magnetic Resonance, Harper and Row, London 1969.
[19] M. S. de Groot, I. A. Hesselman, and J. H. van der Waals, Mol. Phys. **16,** 61 (1969).
[20] A. Grupp, Ph.D. Thesis, Universität Stuttgart 1982.
[21] D. Harer, Ph.D. Thesis, Universität Stuttgart 1969.
[22] V. A. Karachevtsev, Sov. Phys. Solid State **28,** 788 (1986).
[23] D. Gundel, J. Frick, J. Krzystek, J. U. von Schütz, and H. C. Wolf, Chem. Phys. (1989), in press.
[24] C. A. Hutchinson, J. V. Nicholas, and G. W. Scott, J. Chem. Phys. **53,** 1906 (1970).
[25] C. P. Slichter, Principles of Magnetic Resonance, Springer, Berlin 1978.
[26] P. J. F. Verbeek, C. A. van't Hof, and J. Schmidt, Chem. Phys. Letters **51,** 292 (1977).
[27] D. Haarer and H. C. Wolf, Mol. Cryst. Liq. Cryst. **10,** 359 (1970).
[28] W. Vollmann, Chem. Phys. **57,** 157 (1981).
[29] J. U. von Schütz, F. Gückel, W. Steudle, and H. C. Wolf, Chem. Phys. **53,** 365 (1980).
[30] N. S. Dalal, D. Haarer, J. Bargon, and H. Möhwald, Chem. Phys. Letters **40,** 326 (1976).
[31] D. Burger, Diplomarbeit, Universität Stuttgart 1981.
[32] H. B. Levinsky and H. C. Brenner, Chem. Phys. Letters **78,** 177 (1981).
[33] F. C. Bos and J. Schmidt, Mol. Phys. **58,** 561 (1986).
[34] H.-L. Yu and T.-S. Lin, Chem. Phys. Letters **102,** 529 (1983).
[35] C. P. Keijzers and D. Haarer, J. Chem. Phys. **67,** 925 (1977).